The Pacific-Indian Ocean Associated Mode in CMIP5 Models

Minghao Yang, Xin Li*, Weilai Shi, Chao Zhang, Jianqi Zhang

College of Meteorology and Oceanography, National University of Defense Technology, Nanjing, 211101, China

Correspondence to: Xin Li (lixin_atocean@sina.cn)

Abstract. The Pacific-Indian Ocean associated mode (PIOAM), defined as the first dominant mode (empirical orthogonal function, EOF1) of SST anomalies in the Pacific-Indian Ocean between 20°S and 20°N, is the product of the tropical air-sea interaction at the cross-basin scale and the main mode of ocean variation in the tropics. Evaluating the capability of current climate models to simulate the PIOAM and finding the possible factors that affect the simulation results are beneficial to obtain more accurate future climate change prediction. Based on 55-yr the Hadley Centre Global Sea Ice and Sea Surface Temperature (HadISST) dataset and the output data from twenty-one Coupled Model Intercomparison Project (CMIP) phase 5 (CMIP5) models, the PIOAM in these CMIP5 models is assessed. It is found that the explained variance of PIOAM in almost all twenty-one CMIP5 models are underestimated. Although all models reproduce the spatial pattern of the positive sea surface temperature anomaly in the eastern equatorial Pacific well, only one-third of these models successfully simulate the ENSO mode with the east-west inverse phase in the Pacific Ocean. In general, CCSM4, GFDL-ESM2M and CMCC-CMS have a stronger capability to capture the PIOAM than that of the other models. The strengths of the PIOAM in the positive phase in less than one-fifth of the models are slightly stronger, and very close to HadISST dataset, especially in CCSM4. The interannual variation of PIOAM can be measured by CCSM4, GISS-E2-R and FGOALS-s2.

1. Introduction

As early as the 1960s, Bjerkness (1966, 1969) studied the phenomenon of El Niño-Southern Oscillation (ENSO). Since then, the impact of ENSO on global climate has become a major concern in climate research. ENSO in the Pacific Ocean is the strongest interannual signal of global climate change, and has been extensively studied by a large number of scholars, including its occurrence and development mechanism (Wyrtki, 1975; Philander et al., 1984; Suarez and Schopf, 1988; Jin, 1997; Li and Mu, 1999;

Li and Mu, 2000; Li, 2002), its evolution characteristics and its impact on global weather and climate (Bjerknes, 1966; Rasmusson and Wallace, 1983; Ropelewski and Halpert, 1987; Li, 1990; Webster and Yang, 1992; Zhou and Zeng, 2001; Mu and Duan, 2003; Mu et al., 2007; Zheng et al., 2007). At the end of the 20th century, an interannual climate anomaly characterized by a sea surface temperature anomaly (SSTA) of opposing sign in the western and eastern tropical Indian Ocean, known as the Indian Ocean dipole (IOD), was reported by Saji et al. (1999) and Webster et al. (1999) and was catalogued as one of the major ocean-atmosphere coupled phenomena. The SSTA in the tropical Indian Ocean subsequently has been widely studied, and a great deal of literature has discussed the causes and mechanisms of the IOD, as well as its weather and climate impacts (Li and Mu, 2001; Li et al., 2003; Saji and Yamagata, 2003; Cai et al., 2005; Rao et al., 2007; Zheng et al., 2013; Wang and Wang, 2014).

IOD was initially thought to be generated only by independent air-sea interactions in the tropical Indian Ocean, but some studies have suggested that the tropical Indian Ocean SSTA in 1997/1998 was caused by the influence of the ENSO event in the Pacific Ocean on the surface wind field of the Indian Ocean through anti-Walker circulation over the equator, thus causing the SSTA in the Indian Ocean (Yu and Rienecker, 1999). It has also been suggested that the east-west asymmetry anomaly of the Indian Ocean SSTA in 1997/1998 may contain the triggering process of ENSO (Ueda and Matsumoto, 2000). Li et al. (2002) showed that there is a significant negative correlation between the tropical Indian Ocean SSTA dipole event and the Pacific SSTA dipole event (similar to ENSO mode) using statistical analysis. Huang and Kinter (2002) also noted that there was a significant relationship between IOD in the Indian Ocean and ENSO in the Pacific Ocean.

The movements and changes of Earth’s fluids (atmosphere and oceans) have a certain connection, and the change in tropical sea surface temperature (SST) should not be an isolated phenomenon. IOD in the Indian Ocean and ENSO in the Pacific Ocean, both as significant basin-scale signals, are supposed to be closely related and interact with each other. Although the type of relationship between ENSO and IOD has not yet been fully demonstrated, extensive research has shown that both SST and the air-sea systems in the Pacific Ocean and the Indian Ocean are closely linked (Klein and Soden, 1999; Li et al., 2008; Huang and Kinter, 2002; Li et al., 2003; Annamalai et al., 2005; Cai et al., 2019). The Walker circulation anomaly induced by SSTA over the equatorial Pacific Ocean will cause a Walker circulation anomaly over the Indian Ocean, which could inspire the occurrence and development of IOD in the

Indian Ocean driven by abnormal wind stress in the lower layer. On the other hand, Indonesian Throughflow also plays a role in the connection between ENSO and IOD. The cold (El Nino) or warm (La Nina) SST of the warm pool in the Pacific Ocean can cool or warm the SST in the eastern equatorial Indian Ocean through the Indonesian Throughflow, which is conducive to the establishment of a positive or negative phase of IOD.

Yang and Li (2005) found the first leading mode of the tropical Pacific-Indian SSTA reflecting the opposite phase characteristics of both the middle west Indian Ocean and equatorial middle east Pacific Ocean and both the eastern Indian Ocean and equatorial western Pacific Ocean, from which they proposed the concept of the Pacific-Indian Ocean associated mode (PIOAM), and noted that the PIOAM can better reflect the influence of the tropical SSTA on Asian atmospheric circulation. Yang et al. (2006) subsequently found that the influences of the PIOAM and the ENSO mode on summer precipitation and climate in China were very different, and their numerical experiments also showed that the simulation results obtained by considering the PIOAM were more consistent with observation data. Based on multi-variable empirical orthogonal functions, Chen and Cane (2008) and Chen (2011) also found this phenomenon and named it Indo-Pacific Tripole (IPT), which is considered to be an intrinsic mode in the tropical Indo-Pacific Ocean. In addition, Lian et al. (2014) used a conceptual model to discuss the development and physical mechanism of the IPT. By analyzing the monthly thermocline temperature anomaly (TOTA) from 1958-2007 and the weekly sea surface height (SSH) anomaly from 1992-2011 in the tropical Pacific–Indian Ocean, Li et al. (2013) further found that the PIOAM are more obviously in the subsurface ocean temperature anomaly field, especially in the thermocline. Based on the simulation results of the LASG/IAP (State Key Laboratory of Numerical Modeling for Atmospheric Sciences and Geophysical Fluid Dynamics/Institute of Atmospheric Physics) Climate system Ocean Model (LICOM), version 2 (LICOM2.0) (Liu et al. 2012) and observation data, Li and Li (2017) proved that PIOAM is an important tropical Pacific-Indian Ocean SST variation mode that actually exists both in observation and simulation. Therefore, when studying the influence of SSTA in the Pacific and Indian oceans on weather and climate, the Pacific and Indian oceans should be considered as unified.

Since the PIOAM is so important, how well do current climate models simulate it? To answer this question, the outputs from the climate system models for the Coupled Model Intercomparison Project (CMIP) phase 5 (CMIP5) were used for this research, from which we aim to provide a more complete evaluation of the PIOAM and try to find possible reasons that cause the simulation biases. In the following, Sect. 2 includes a brief description of the HadISST dataset, CMIP5 models, and the methods used in this study. Section 3 presents the assessments of the PIOAM in the CMIP5 models. A conclusion and discussion are given in Sect. 4.

2. Data and methods

The SST data from the Hadley Centre Global Sea Ice and Sea Surface Temperature (HadISST) (Rayner et al., 2003) dataset is used for this study. The data are monthly averaged data from 1951 to 2005 with a spatial resolution of 1°×1°. Brief information for the 21 CMIP5 models for the historical period used in this article is provided in Table 1. It's worth noting that some models have higher resolution in tropics. Considering that output data resolutions vary between the models, we first interpolated all data into a 1°×1° grid to facilitate comparison between the models and HadISST dataset.

Table 1. List of 21 selected CMIP5 climate models.

Model name	Modeling group	Oceanic resolution (lon×lat)
CanESM2 (Second Generation Canadian Earth System Model)	Canadian Centre for Climate Modeling and Analysis, Canada	256×192
CCSM4 (The Community Climate System Model, version 4)	NCAR, USA	320×384
CMCC-CESM (Centro Euro-Mediterraneo sui Cambiamenti Climatici (CMCC) Carbon Earth System Model)	CMCC, Italy	182×149
CMCC-CM (CMCC Climate Model)	CMCC, Italy	182×149
CMCC-CMS (CMCC-CM with a resolved stratosphere)	CMCC, Italy	182×149
CNRM-CM5 (Centre National de Recherches Météorologiques (CNRM) Coupled Global Climate Model, version 5)	CNRM, France	362×292
FGOALS-s2 (The Flexible Global Ocean-Atmosphere-Land System model, Spectral Version 2)	LASG, China	360×196
GFDL-ESM2M (Earth System Model of Geophysical Fluid Dynamics Laboratory (GFDL) with Modular Ocean Model, version 4)	GFDL, USA	144×90
GISS-E2-H (Goddard Institute for Space Studies (GISS) Model E version 2 (GISS-E2) with HYCOM ocean model)	NASA, USA	144×90
GISS-E2-H-CC (GISS-E2-H with carbon cycle)	NASA, USA	144×90
GISS-E2-R (GISS-E2 with Russell ocean model)	NASA, USA	144×90
GISS-E2-R-CC (GISS-E2-R with carbon cycle)	NASA, USA	144×90
HadCM3 (the third version of he Hadley Centre coupled model)	Met Office Hadley Centre, UK	288×144
HadGEM2-AO (Hadley Global Environment Model 2 (HadGEM2)-Atmosphere-Ocean)	Met Office Hadley Centre, UK	360×216
HadGEM2-CC (HadGEM2-Carbon Cycle)	Met Office Hadley Centre, UK	360×216

HadGEM2-ES (HadGEM2-Earth System)	Met Office Hadley Centre, UK	360×216
IPSL-CM5B-LR (Institut Pierre Simon Laplace Climate Model 5B (LPSL-CM5B)-Low Resolution)	IPSL, France	182×149
IPSL-CM5B-MR (LPSL-CM5B 5A-Medium Resolution)	IPSL, France	182×149
MIROC-ESM (Model for Interdisciplinary Research on Climate, Earth System Model)	Atmosphere and Ocean Research Institute (AORI), Japan	256×192
MIROC-ESM-CHEM (An atmospheric chemistry coupled version of MIROC-ESM)	AORI, Japan	256×192
NorESM1-M (Norwegian Climate Centre Earth System Model)	Norwegian Climate Centre, Norway	384×320

The PIOAM is determined according to the method of Ju et al. (2004) and Li et al. (2018), that is, the first leading mode (empirical orthogonal function, EOF1) of the tropical Pacific-Indian ocean SSTA (20°S-20°N, 40°E-80°W) is used to represent the PIOAM. The annual cycle and the linear trend are removed to obtain the monthly SSTA. Ju et al. (2004) used this method to analyze SSTA in the tropical Pacific-Indian Ocean in different seasons, and found the existence of PIOAM in all seasons with a contribution to total variance of more than 33%, indicating that the spatial distribution structure of PIOAM was stable.

Accounting for the intimate connection between the Pacific ENSO mode and the Indian Ocean dipole, Yang et al. (2006) argued that the PIOAM index (PIOAMI) can be defined as the respectively normalized east-west SSTA differences of the equatorial areas in the two oceans. As to the SSTA, the SSTA of ENSO is stronger than that in the equatorial Indian Ocean because of the larger Pacific basin; however, as to the influence of the SSTA on East Asia, a series of numerical experiments clearly indicate that the effect of SSTA forcing on the Indian Ocean is stronger than that of the eastern equatorial Pacific (Shen et al., 2001; Guo et al., 2002; Guo et al., 2004; Yang et al., 2006). Therefore, the PIOAMI is defined on the basis of the respective normalized dipoles in the Pacific and the Indian Ocean. According to the method of Yang et al. (2006), The PIOAMI is defined as follows:

$$\mathrm{PIOAMI} = \mathrm{IOI} + \mathrm{POI} \quad (1)$$

$$\mathrm{IOI} = \mathrm{SSTA}(5°\mathrm{S} - 10°\mathrm{N},\ 50°\mathrm{E} - 65°\mathrm{E}) - \mathrm{SSTA}(10°\mathrm{S} - 5°\mathrm{N}, 85°\mathrm{E} - 100°\mathrm{E}) \quad (2)$$

$$\mathrm{POI} = \mathrm{SSTA}(5°\mathrm{S} - 5°\mathrm{N},\ 130°\mathrm{W} - 80°\mathrm{W}) - \mathrm{SSTA}(5°\mathrm{S} - 10°\mathrm{N}, 140°\mathrm{E} - 160°\mathrm{E}) \quad (3)$$

where IOI and POI are the normalized Indian Ocean and Pacific Ocean indeices, respectively.

3. Results

3.1 Spatial pattern

Figure 1 shows the pattern of SST anomalies over the Indo-Pacific Ocean in October 1982 and September 1997. It can be clearly seen that there are obvious warm tongues in the eastern equatorial Pacific Ocean, obvious positive SST anomalies in the northwest Indian Ocean, and obvious negative SST anomalies in the western equatorial Pacific Ocean and the eastern Indian Ocean. This is precisely the typical spatial pattern characteristics of the PIOAM mentioned above. That is to say, the SST anomalies in the northwest Indian Ocean and the equatorial middle-east Pacific Ocean is opposite to the SST anomalies in the western equatorial Pacific Ocean and the east Indian Ocean. Compared with ENSO and IOD, the PIOAM has a broader spatial distribution.

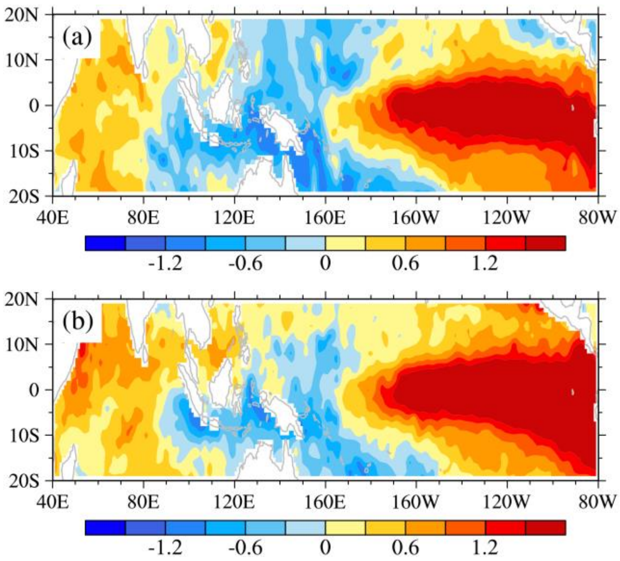

Figure 1: Maps of SST anomalies for (a) October 1982 and (b) September 1997 from the HadISST dataset (unit: °C). The period from 1981 to 2005 is used to extract the monthly SST climatology.

However, is this spatial pattern of SST anomalies only a special case of a certain year, or is it stable? To answer this question, EOF analysis is performed on the SST anomalies of different seasons over Indo-Pacific Ocean (20°S-20°N, 40°E-80W°) from 1951 to 2005. All these first leading modes in Fig. 2 are well separated from the remaining leading modes, based on the criteria of North et al. (1982), which means less likely to be affected by statistical sampling errors. It can be found that the patterns of summer (June, July and August; Fig. 2.b) and autumn (September, October and November; Fig. 2.c) display the typical spatial distribution of the PIOAM, with the 46% and 61% contribution to total variance, respectively, while the spatial pattern of PIOAM is not so obvious in spring (March, April and May; Fig. 2.a) and winter (December, January and February; Fig. 2.d). In general, the PIOAM has stable structure and practical significance, especially in autumn.

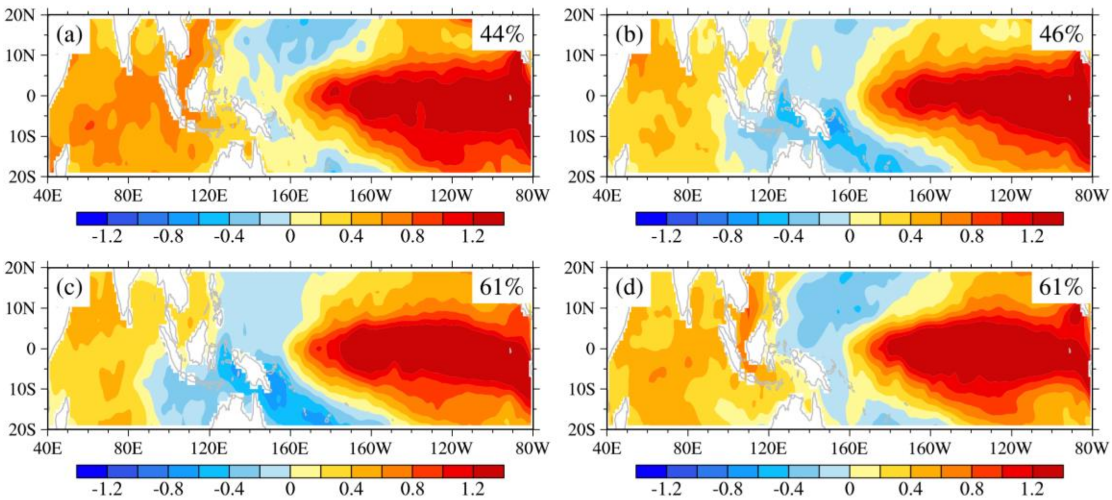

Figure 2: Spatial patterns of the first leading mode of the (a) spring (March, April and May), (b) summer (June, July and August), (c) autumn (September, October and November) and (d) winter (December, January and February) averaged SST anomalies over Indo-Pacific Ocean (20°S-20°N, 40°E-80W°) calculated from HadISST dataset (unit: °C). The numbers at the upper right corner of each panel indicate the percentage of variance explained by each season.

Performing the EOF analysis on the monthly SST anomalies regardless of seasonal differences, Figure 3 depicts the spatial pattern of PIOAM in the selected 21 CMIP5 models and their differences compared to HadISST dataset (Fig. 3a). Figure 3.b shows the results of a multi-model ensemble (MME) that represents the mean of the results from all selected models. The PIOAM in HadISST dataset and CMIP5 models is well separated from the second leading mode, according to the criterion of North et al. (1982). To better and objectively evaluate the capability of each model in simulating PIOAM, a Taylor diagram (Fig. 4) is also adopted to concisely display the relative information from multiple models, so that the differences among the simulations from all models are revealed clearly (Taylor, 2001; Jiang and Tian, 2013; Yang et al., 2018). According to HadISST dataset (Fig. 3.a), with a 47% contribution to total variance, the PIOAM has a warm tongue spatial pattern in the eastern equatorial Pacific Ocean, whereas there is negative SSTA in the western equatorial Pacific Ocean, which exhibits an obvious ENSO mode in the Pacific Ocean. In addition, there are obvious positive SSTA in the western Indian Ocean region of the PIOAM, but the SSTA in the eastern equatorial Indian Ocean region remain positive. Considering that the IOD is defined by the difference between the SSTA in the western equatorial Indian Ocean and that in the eastern equatorial Indian Ocean, this indicates zonal surface heat contrast of the Indian Ocean SSTA. Although it is called a dipole, it is also like a meridional seesaw (Li et al., 2002; Yang et al., 2006). Therefore, it can be considered that the PIOAM represents an IOD mode in the Indian Ocean region.

Figure 3 shows that all of these models can generally reproduce the spatial pattern of PIOAM, yet large discrepancies exist regarding the strength, and the differences between the models are also significant. Except for the contribution to total variance of PIOAM in CCSM4 and CMCC-CESM are nearly consistent with HadISST dataset, the variance contribution of PIOAM in almost all CMIP5 models are lower than those in the HadISST dataset, especially CMCC-CM with a contribution to total variance as small as 26%. In terms of strength, it is apparent that the simulation errors of these models are mainly concentrated in the Pacific Ocean compared to the Indian Ocean. Compared to the HadISST dataset, a majority of models overestimate the strength of PIOAM in the equatorial east Pacific and central Pacific; only one-seventh of the models (IPSL-CM5A-LR, IPSL-CM5A-MR and MIROC-ESM) underestimate the strength of PIOAM in the equatorial east Pacific, while the simulation results of HadGEM2-AO and CMCC-CM in the equatorial central Pacific and western Pacific are weak. The simulation errors of the strength of the ENSO-like mode in CCSM4, CMCC-CMS, GFDL-ESM2M and GISS-E2-R-CC are lower than those in other models. For the Indian Ocean, the strengths of PIOAM in only approximately one-quarter of the models (CanESM2, CMCC-CESM, GISS-E2-H-CC, HadCM3 and HadGEM2-AO) are basically consistent with HadISST dataset with small simulation errors. Nearly half of the models were smaller for the eastern Indian Ocean, whereas more than half were larger for the western Indian Ocean. In general, the simulation error in the Indian Ocean region is significantly smaller than that in the Pacific region. According to Fig. 4, it is apparent that the root mean square errors (RMSEs) in MIROC-ESM-CHEM, IPSL-CM5A-LR and MIROC-ESM are relatively large, which means that the capabilities of these modes to simulate the strength of PIOAM are still inadequate, whereas the RMSEs in CCSM4, CMCC-CMS and GFDL-ESM2M are smaller than in other models with a better performance. In addition, as shown in Fig. 3.b, MME better simulates the amplitude of PIOAM in the Indian Ocean than most these selected CMIP5 models with smaller simulation errors, but the amplitude in the equatorial Pacific are larger than that of the HadISST dataset.

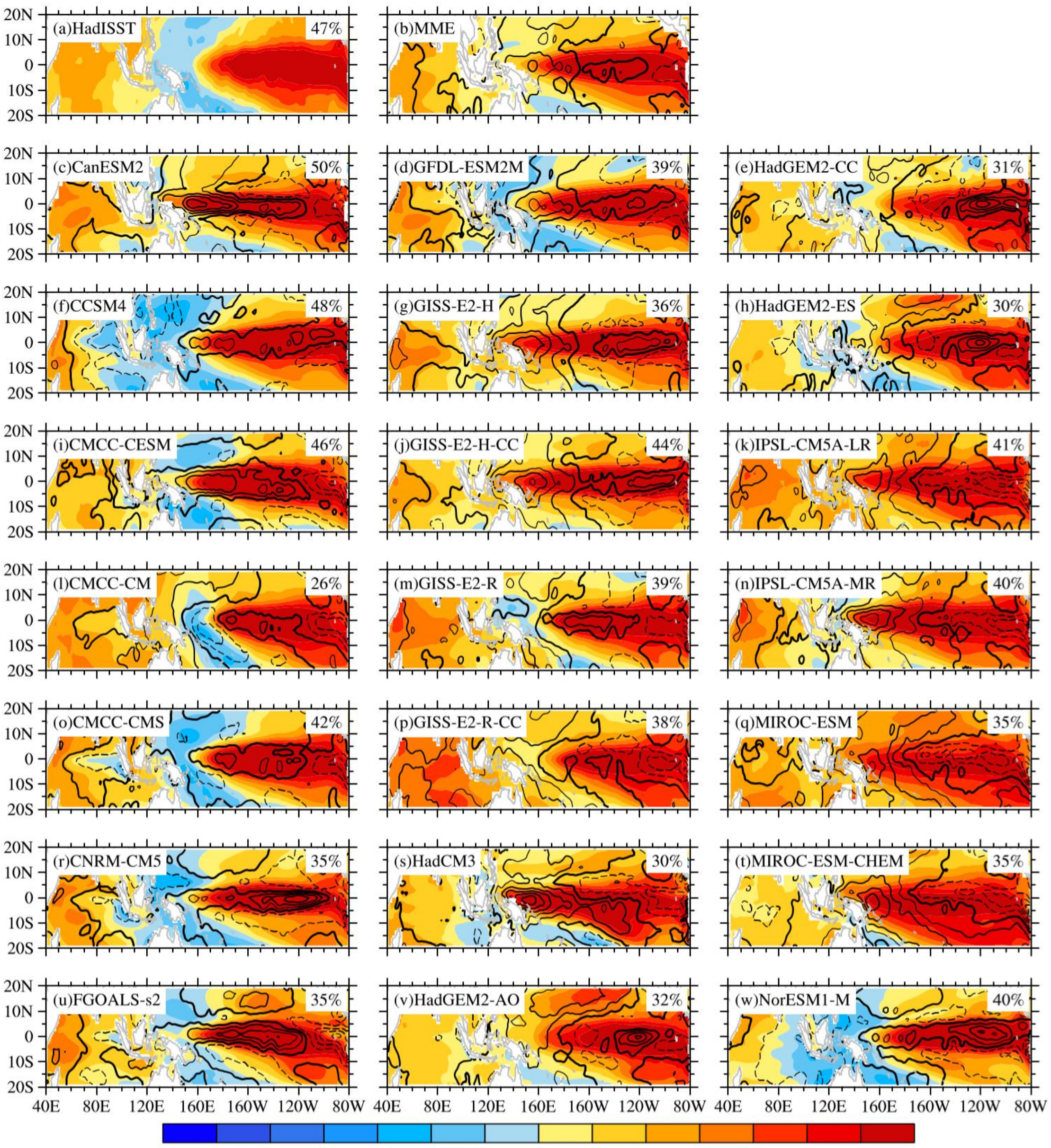

Figure 3: PIOAM (shading) and the difference between each model and HadISST dataset (contour, with an interval of 0.3, shown as black bold lines represent the contour with the zero value, dashed contours denote negative values, unit: ℃). The numbers at the upper right corner of each panel indicate the percentage of variance explained by each model.

As for spatial patterns, the IOD-like mode in the Indian Ocean region can be simulated in almost all models except MIROC-ESM-CHEM. Although all these models reproduce the spatial pattern of the positive SSTA well in the eastern equatorial Pacific, only one-third of the models (CCSM4, CMCC-CM, CMCC-CMS, CNRM-CM5, FGOALS-s2, GFDL-ESM2M and NorESM1-M) successfully simulate the ENSO-like mode with the east-west inverse phase in the Pacific Ocean. In addition, the simulated positive SSTAs in the eastern equatorial Pacific in HadCM3 and MIROC-ESM-CHEM are further south.

According to Fig. 4, more than one-third of these models (CCSM4, CMCC-CMS and GFDL-ESM2M, etc.) can simulate the spatial pattern of PIOAM well, and the spatial correlation coefficients between these models and the HadISST dataset are all greater than 0.9, especially CCSM4, which is as high as 0.95. In contrast, the spatial pattern of PIOAM in MIROC-ESM-CHEM is unsatisfactory with a spatial correlation coefficient of only 0.69. The simulation results of HadCM3 and MIROC-ESM are also relatively poor, and the spatial correlation coefficients with HadISST dataset are less than 0.8. It can also be learned from Fig. 4 that, for the standard deviation of PIOAM, very large differences exist among these models. The standard deviations of PIOAM in IPSL-CM5A-LR, MIROC-ESM and GISS-E2-R-CC are quite different from those of the HadISST dataset, while the simulation results of CMCC-CMS, GFDL-ESM2M and HadGEM2-CC are basically close to those of the HadISST dataset and have better performance. It is noteworthy that the standard deviations of PIOAM in more than half of these models are smaller than that of the HadISST dataset, and their differences are large. Although the spatial pattern of PIOAM in MME is closer to the HadISST dataset and the RMSE is smaller than the vast majority of single models, the standard deviation of PIOAM in MME is smaller than that of the HadISST dataset.

In general, CCSM4, GFDL-ESM2M and CMCC-CMS have a stronger ability to simulate the PIOAM. In addition, although the MME may not be as good as that of a single model in some specific aspects, overall, considering spatial pattern, standard deviation and RMSE, MME is still superior to most single models.

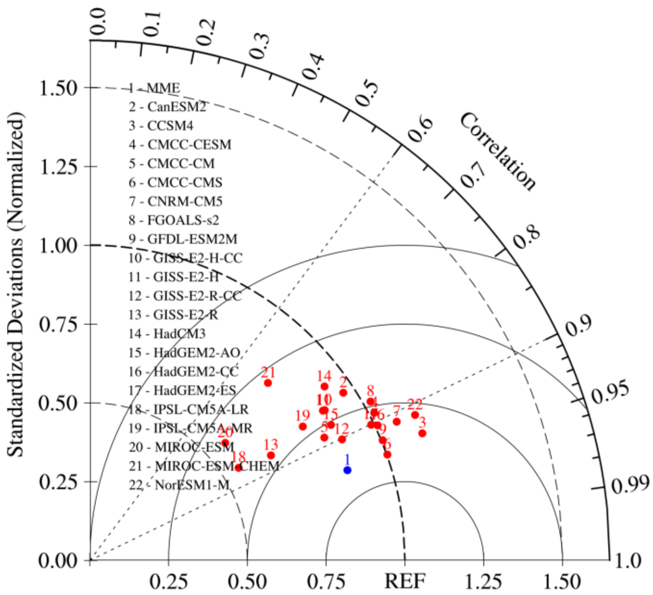

Figure 4: Taylor diagram of PIOAM.

To further evaluate the differences between these models, Fig. 5 shows the distribution of standard deviations between the CMIP5 models, which clearly reflects the regional differences between the models. It is apparent that the differences are mainly concentrated in the eastern equatorial Pacific. Therefore, the emphasis of improving the model on simulating the PIOAM is to improve the capability of the model to simulate to the Eastern-Pacific (EP) type ENSO.

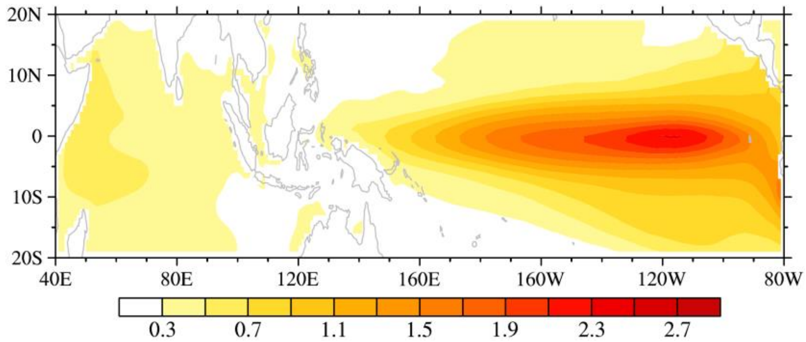

Figure 5: The standard deviations of simulated PIOAM between the selected 21 CMIP5 models (unit: °C).

3.2 PIOAM index

3.2.1 Time series

A satisfactory index is needed to describe the PIOAM. It is customary to select the time coefficient (PC1) of the PIOAM as its index. It can be seen from the regression of the monthly SSTA onto the normalized PC1 (Fig. 6.a) that the pattern in the Pacific Ocean is similar to ENSO, but positive SST anomalies occur throughout the Indian Ocean, which not matches the typical PIOAM spatial pattern. This is because the ENSO signals in the Pacific Ocean in PC1 are so strong that the signals of the IOD are not fully reflected. The correlation coefficient between PC1 and Niño3.4 index is as high as 0.95. However, obvious negative SST anomalies in the eastern Indian Ocean can be found in the regression map of the monthly SSTA based on the normalized PIOAMI defined in Section 2. The correlation coefficient between PIOAMI and Niño3.4 index is 0.68, indicating PIOAMI contains more Indian Ocean signals than PC1. In addition, the correlation coefficient between PC1 and PIOAMI is 0.70, which is far more than the confidence level of 99%. Therefore, PIOAMI can describe the mode well because of giving consideration to both the signals in the Pacific Ocean and the signals in the Indian Ocean.

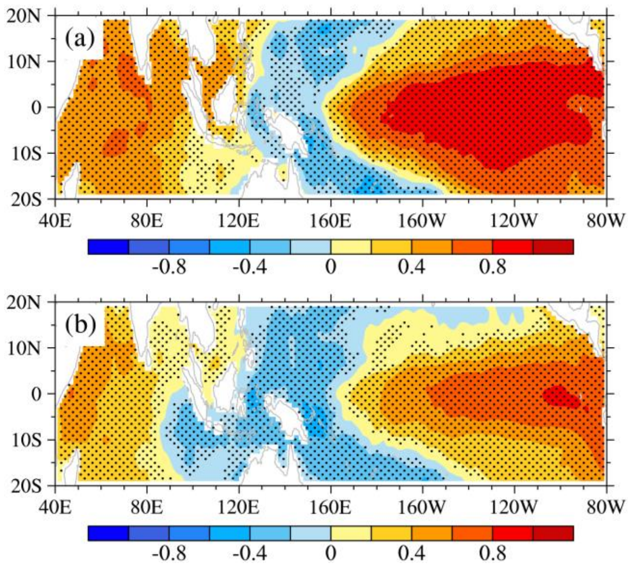

Figure 6: Regressions of the monthly SSTA onto the normalized (a) PC1 and (b) PIOAMI for the period from 1951 to 2005 (unit: ℃). The stippled areas for SSTA denote the 99% confidence levels.

Figure 7. shows the monthly time series of the PIOAMI, Pacific Ocean index (POI) and Indian Ocean index (IOI) from 1951 to 2005. The wavelet analysis of PIOAMI indicates that PIOAM has obvious seasonal and interannual variations, as well as interdecadal variations (feature is omitted). According to Fig. 7, POI and IOI have the same variation tendency at most times, thus the PIOAMI amplitude is greatly enhanced. However, there are a few cases where the two change in opposing ways, resulting in a much weaker PIOAMI. Moreover, from the time-series of PIOAMI, there is an interannual oscillation of positive and negative phases in the PIOAM, and there is also a phenomenon that the PIOAMI is very weak or not obvious in some years.

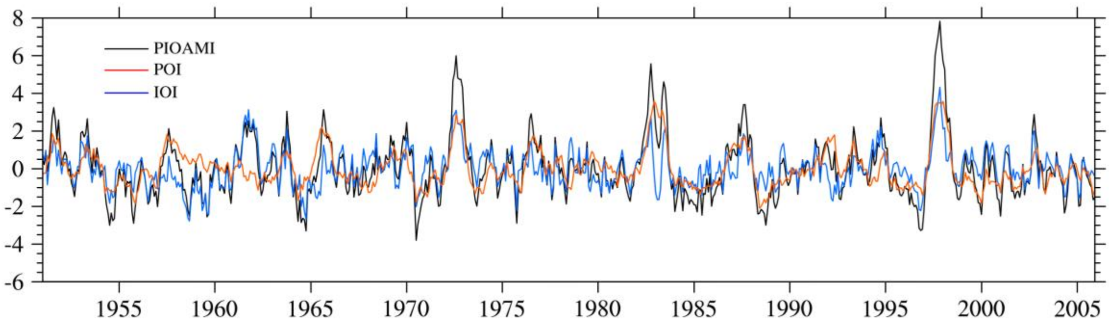

Figure 7: Time-series of PIOAM index (black), Pacific Ocean index (red) and Indian Ocean index (blue) in the HadISST dataset.

Considering that the PIOAM mainly reaches its peak in autumn (September, October and

November), we select the year with significant positive and negative phases of PIOAM by taking one standard deviation as the criterion, and calculate the difference of autumn PIOAMI between each CMIP5 model and the HadISST dataset (see Fig. 8) to further reveal the simulation of the CMIP5 models on the strength of the PIOAM. As shown by Fig. 8.a, the simulated strengths of the PIOAM in the positive phase are underestimated in most models, whereas they are slightly overestimated in less than one-fifth of the models (CCSM4, CMCC-CMS, CNRM-CM5 and GFDL-ESM2M) are slightly stronger, which are very close to the HadISST dataset, especially in CCSM4. However, nearly half of the models overestimate the strength of the PIOAM in the negative phase (Fig. 8.b), in which the simulation results of CanESM2 and GISS-E2-R are consistent with the HadISST dataset. Although CCSM4 has a better performance in simulating the strength of the PIOAM in the positive phase than other models, the simulation error of the negative phase is very large.

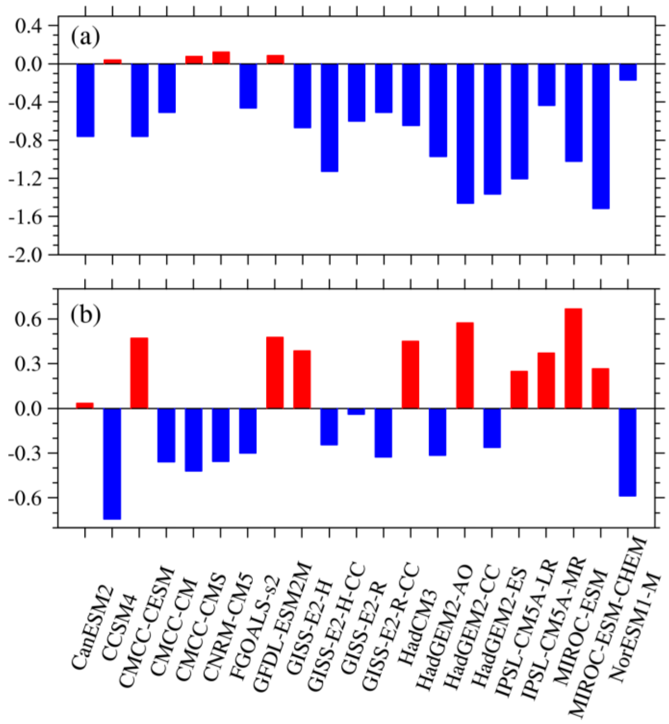

Figure 8: Difference in the amplitude of the PIOAMI in the positive phase (a) and negative phase (b) between the CMIP5 models and HadISST dataset.

According to PIOAM positive and negative phase year based on the autumn PIOAMI, SSTAs in the tropical Pacific-Indian Ocean in October are composited to obtain the spatial pattern of SSTAs in the PIOAM positive and negative phases. It is clear in Fig. 9 that the SSTAs in the Pacific-Indian Ocean in both the MME of CMIP5 models and HadISST dataset present patterns with a tripole structure, where the Indian Ocean is represented by the IOD-like mode and the Pacific Ocean by the ENSO-like mode, which again demonstrates the authenticity of PIOAM and the rationality of PIOAMI used in this article.

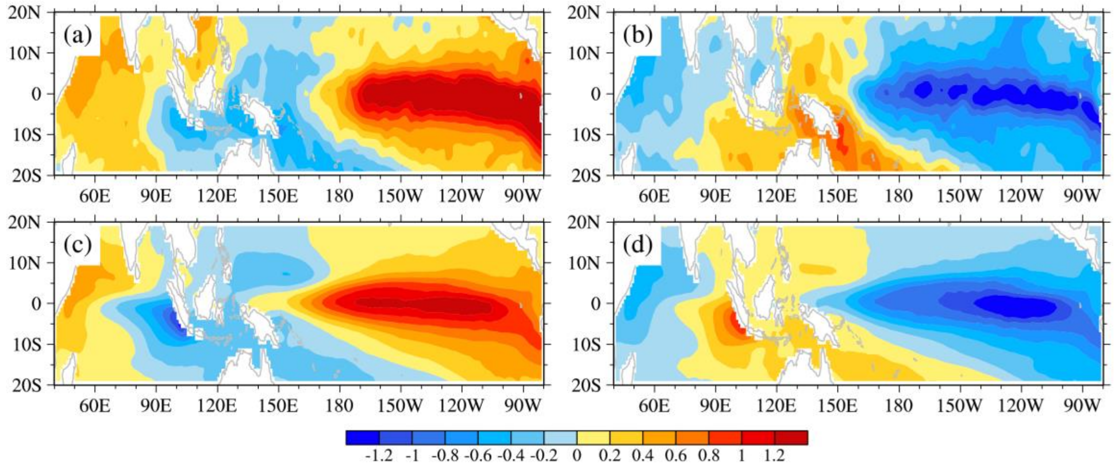

Figure 9: The tropical Pacific-Indian Ocean SSTAs of the PIOAM positive (a, c) and negative (b, d) phase in October in the HadISST dataset (a, b) and the MME of CMIP5 models (c, d) (unit: °C).

3.2.2 Interannual Variation of PIOAM

To evaluate the ability of these CMIP5 models to simulate the interannual variation of PIOAM, Fig. 10 shows the ratios of standard deviation of IOI, POI and PIOAMI in autumn in each model to those in the HadISST dataset. The closer the ratio is to 1, the better the ability to simulate interannual variation. It can be found that the difference in the simulation results of the interannual variation of PIOAMI among these models is smaller compared to IOI and POI. The simulation results of CCSM4, GISS-E2-R and FGOALS-s2 are almost consistent with HadISST dataset, indicating that these three models have relatively strong capabilities to simulate the interannual variation of PIOAM. Except that NorESM1-M overestimates the interannual variation of PIOAM, the simulation results in most of the models are weak, especially MIROC-ESM, which leads to MME underestimating the interannual variation of PIOAM compared to the HadISST dataset. In addition, the interannual variations of IOI in GFDL-ESM2M, GISS-E2-R-CC and CMCC-CM are better than other models, whereas the simulation results are underestimated in most models. In contrast to IOI, the vast majority of models overestimate the interannual variations of POI, and the simulated interannual variations of POI in only three models (IPSL-CM5A-MR, CMCC-CESM and IPSL-CM5A-LR) are weaker than the HadISST dataset. Based on the above analysis, it is apparent that the interannual variation of PIOAMI is more closely to IOI than POI, and the interannual variation of PIOAM in autumn can be measured by CCSM4, GISS-E2-R and FGOALS-s2.

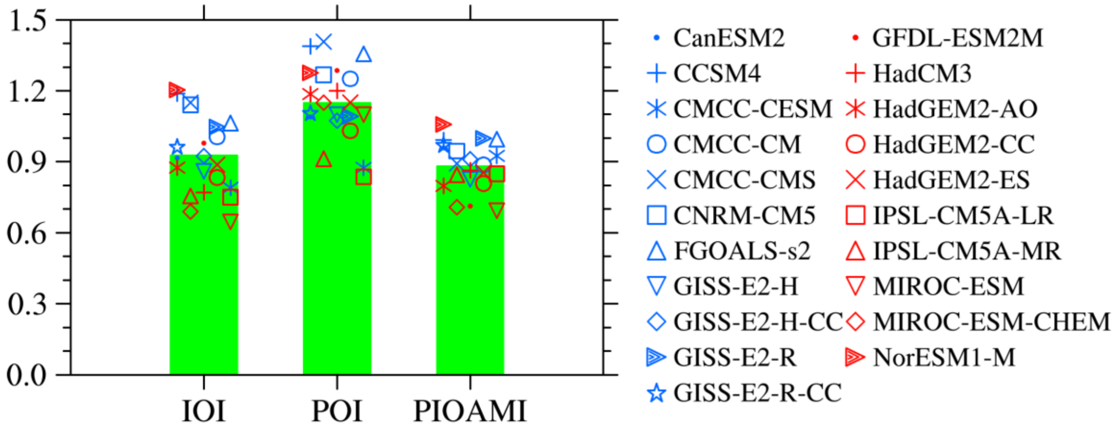

Figure 10: Ratios of standard deviation of autumn IOI, POI and PIOAMI in each model to those in the HadISST dataset. Green bar represents the MME of the corresponding index.

3.2.3 The relationship of PIOAM with ENSO and IOD

The lag-lead correlation analysis between PIOAMI and the Niño3.4 index derived from the HadISST dataset shows that PIOAM has a close correlation with the ENSO mode at the same period and one month lagging with the correlation coefficient of 0.68 (Fig. 11.a). In addition, PIOAM and IOD also have a close correlation in the same period, with a correlation coefficient of 0.73 (Fig. 11.b), indicating that the PIOAM can reflect the activities of ENSO in the Pacific Ocean and IOD in the Indian Ocean to a considerable extent. It should be noted that the IOD index used in this research is according to the definition of Saji et al. (1999), i.e. the difference in SSTA between the tropical western Indian Ocean (50°E-70°E, 10°S-10°N) and the tropical south-eastern Indian Ocean (90°E-110°E, 10°S-0). In these CMIP5 models, more than one-half of the models successfully reproduce the maximum correlation between PIOAM and ENSO in the same period. The correlation coefficients of the PIOAMI and the Niño3.4 index in HadGEM2-AO and HadGEM2-ES are both 0.68, which is consistent with the HadISST dataset, and the correlation coefficients of FGOALS-s2, GISS-E2-H and GISS-E2-H-CC are 0.69, 0.69 and 0.70, respectively. However, the correlation coefficients of MIROC-ESM and MIROC-ESM-CHEM are only 0.37 and 0.30, which are significantly different from the results of the HadISST dataset and other models, indicating that the two models cannot simulate the close relationship between the PIOAM and ENSO well. In addition, the correlation coefficient of PIOAMI and the Niño3.4 index in MME is 0.66, which is slightly lower than the HadISST dataset but shows the close contemporaneity correlation between the PIOAM and ENSO; the overall change of the correlation coefficient series is very close to the HadISST dataset.

For the relationship between the PIOAM and IOD, it is apparent from the HadISST dataset in Fig. 11.b that the PIOAM and IOD show obvious close correlation in the same period, and the correlation coefficient is as high as 0.73. It is satisfactory that all selected CMIP5 models successfully reproduce the correlation between PIOAM and IOD in the same period, but the simulation results in more than half of them are underestimated. Among these models, the simulation results of HadGEM2-ES and GIS-E2-R-CC are basically consistent with the HadISST dataset, which shows that the two models have stronger capability to simulate the relationship between PIOAM and IOD.

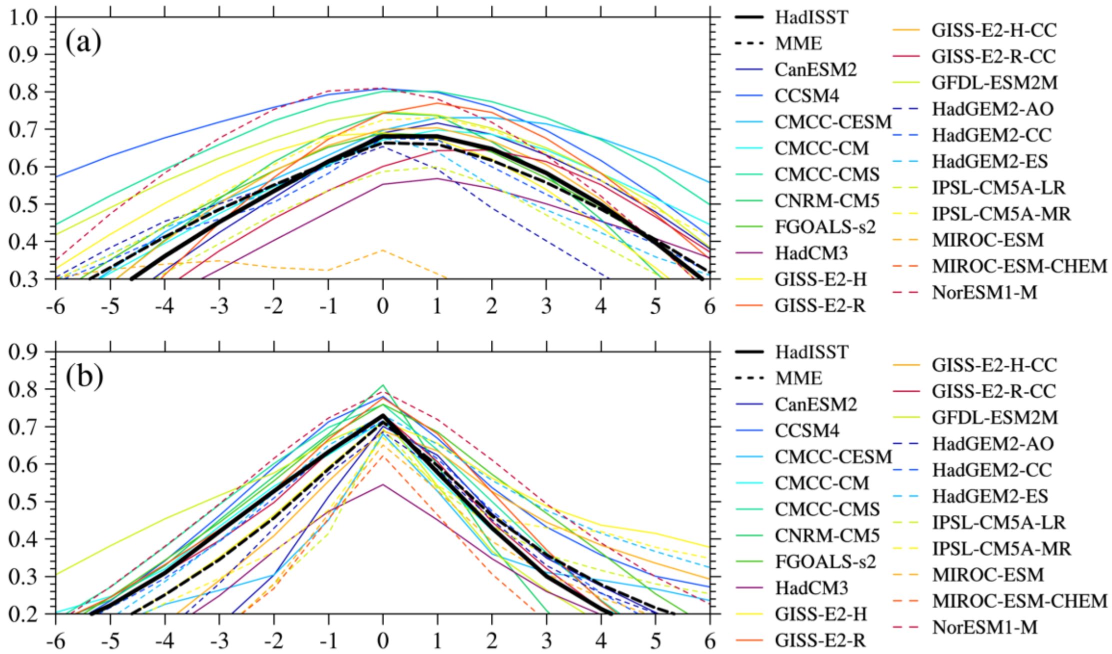

Figure 11: The lag-lead correlation coefficient of the PIOAMI with the Niño3.4 index (a) and IOD index (b). Ordinate represents the correlation coefficient, and abscissa is the lag in months: positive (negative) for the Niño3.4 index or IOD index (PIOAMI) leading PIOAMI (Niño3.4 index or IOD index)

4. Conclusion and discussion

Based on HadISST dataset from 1951 to 2005, the Pacific-Indian Ocean associated mode, proposed by Yang and Li (2005) is evaluated for 21 CMIP5 models. This research provides a relatively comprehensive evaluation of the spatial pattern, the interannual variation and the relationship with ENSO and IOD of the PIOAM in the selected CMIP5 models. The main conclusions are as follows.

With a 47% contribution to total variance, the spatial pattern of PIOAM in the eastern equatorial Pacific Ocean is a warm tongue, whereas there is negative SSTA in the western equatorial Pacific Ocean that exhibits an obvious ENSO mode in the Pacific Ocean. In addition, the PIOAM presents an IOD mode in the Indian Ocean. The variance contributions of PIOAM in almost all CMIP5 models are smaller than that in the HadISST dataset. The simulation errors and differences among these models are mainly concentrated in the Pacific Ocean, compared to the Indian Ocean, and a majority of models overestimate the strength of PIOAM in the equatorial east Pacific and central Pacific. Although all these models reproduce the spatial pattern of the positive SSTA in the eastern equatorial Pacific well, only one-third of the models (CCSM4, CMCC-CM, CMCC-CMS, CNRM-CM5, FGOALS-s2, GFDL-ESM2M and NorESM1-M) successfully simulate the ENSO mode with the east-west inverse phase in the Pacific Ocean. In general, CCSM4, GFDL-ESM2M and CMCC-CMS have stronger capability to simulate the PIOAM than the other models.

The PIOAM is very weak or not obvious in some years and has obvious seasonal and interannual variations, as well as interdecadal variations. The simulated strengths of the PIOAM in the positive phase are underestimated in most models; only less than one-fifth of the models (CCSM4, CMCC-CMS, CNRM-CM5 and GFDL-ESM2M) are slightly stronger, and very close to the HadISST dataset, especially CCSM4. The interannual variation of PIOAM in CCSM4, GISS-E2-R and FGOALS-s2 are almost consistent with the HadISST dataset. Except that NorESM1-M overestimate the interannual variation of PIOAM, the simulation results in most models are weak, especially MIROC-ESM. The interannual variation of PIOAM in autumn can be measured by CCSM4, GISS-E2-R and FGOALS-s2. The PIOAM can well reflect the activities of ENSO in the Pacific Ocean and IOD in the Indian Ocean to a considerable extent with a close correlation to ENSO and IOD for the same period, as well as one month in advance with ENSO.

It is undoubtedly difficult to directly find the factors that influence the model to simulate the PIOAM. The simulation results of model families, such as CMCC, IPSL, MIROC, GISS and HadGEM2, provide clues and comparative data to find the possible reasons that may lead to simulation differences. However, it needs in-depth analysis which is supported by a large number of models, or by dedicated experiments.

Yang et al. (2006) found that only considering the ENSO in the Pacific cannot entirely explain the influence of SSTA on climate variation, and suggested that, to provide better scientific explanation for short-term climate prediction, the PIOAM and its influence should be considered and investigated. In addition, a review article by Cai et al. (2019) provides the first comprehensive review and summary of the current research advances in the interaction between the tropical Pacific-Indo-Atlantic climate systems, and they pointed out that an in-depth understanding of the dynamic mechanisms of intertropical basin interactions is an important way to improve the ability of seasonal to decadal climate prediction. Therefore, evaluating and improving the capability of current climate models to simulate the PIOAM and even the tropical Pacific-Indo-Atlantic climate systems are beneficial to obtain accurate climate change predictions. In addition, improving the level of climate prediction is not only helpful to grasp the changes in the ocean environment of the Pacific-Indian Ocean, but also propitious to improve the ability of prediction and assessment of ocean waves and wind energy (Zheng and Li, 2015; Zheng and Li, 2017).

Data availability. The CMIP5 data are available at https://esgf-node.llnl.gov/search/cmip5/. The sea surface temperature are available at https://www.metoffice.gov.uk/hadobs/hadisst/data/download.html

Author contributions. Xin Li and Weilai Shi conceived the idea and designed the structure of this paper; Minghao Yang performed the experiments; Minghao Yang, Chao Zhang and Jianqi Zhang analyzed the data; Minghao Yang wrote the paper.

Competing interests. The author declares that they have no conflict of interest.

Author Contributions. This research was supported by National Natural Science Foundation of China (4160501, 41490642, 41520104008).

References:

Annamalai, H., Xie, S. P., Mccreary, J. P. and Murtugudde, R.: Impact of Indian Ocean Sea Surface Temperature on Developing El Niño. J. Clim., 18(1), 302-319, doi:10.1175/jcli-3268.1, 2005.

Bjerknes, J.: A possible response of the atmospheric Hadley circulation to equatorial anomalies of ocean temperature, Tellus., 18(4), 820-829, doi:10.3402/tellusa.v18i4.9712, 1966.

Bjerknes, J.: Atmospheric teleconnections from the equatodal Pacific, Mon. Wea. Rev., 97(3), 163-172, doi:10.1175/1520-0493(1969)097<0163:atftep>2.3.co;2, 1969.

Cai, W. J., Hendon, H. H. and Meyers, G.: Indian Ocean dipolelike variability in the CSIRO Mark 3 coupled climate model, J. Climate, 18(10), 1449-1468, doi: 10.1175/jcli3332.1, 2005.

Chen, D., Cane, M. A.: El Niño prediction and predictability, J. Comput. Phys., 227, 3625-3640, doi: 10.1016/j.jcp.2007.05.014, 2008.

Chen, D.: Indo-Pacific Tripole: An intrinsic mode of tropical climate variability, Adv. Geosci., 24, 1-18, doi: 10.1142/9789814355353_0001, 2011.

Cai, W., Wu, L., Lengaigne, M., Li, T., McGregor, Shayne., and et al.: Pantropical climate interactions, Science, 363(eaav4236), doi: 10.1126/science.aav4236, 2019.

Guo, Y. F., Zhao, Y. and Wang, J.: Numerical simulation of the relationships between the 1998 Yangtze River valley floods and SST anomalies, Adv Atmos Sci, 19(3), 391-404, doi:10.1007/s00376-002-0074-0, 2002.

Guo, Y. F.: Numerical simulation of the 1999 Yangtze River valley heavy rainfall including sensitivity experiments with different anomalies, Adv Atmos Sci, 19(3), 391-404, doi: 10.1007/BF02915677, 2004.

Huang, B. H. and Kinter, J. L.: Interannual variability in the tropical Indian Ocean, J. Geophys. Res., 107(C11): 3199. doi:10.1029/2001JC001278, 2002.

Jin, F. F.: An equatorial ocean recharge paradigm for ENSO. Part I: Conceptual model, J. Atmos. Sci., 54(7), 811-829, doi:10.1175/1520-0469(1997)054<0811:aeorpf>2.0.co;2, 1997.

Ju, J. H., Chen, L. L. and Li, C. Y.: The preliminary research of Pacific-Indian Ocean sea surface tempertature anomaly mode and the definition of its index, Journal of Tropical Meteorology (in chinese), 20(6), 617-624, 2004.

Jiang, D. B. and Tian, Z. P.: East Asian monsoon change for the 21st century: results of CMIP3 and CMIP5 models, Chinese Science Bulletin, 58(12), 1427-1435, doi:10.1007/s11434-012-5533-0, 2012.

Klein, S. A. and Soden, B. J.: Remote sea surface temperature variation during ENSO: evidence for a tropical atmospheric bridge, J. Clim., 12(4), 917-932, doi:10.1175/1520-0442(1999)012<0917:rsstvd>2.0.co;2, 1999.

Li, C. Y. Interaction between anomalous winter monsoon in East Asia and El Niño events, Adv. Atmos. Sci., 7(1), 36-46, doi:10.1007/bf02919166, 1990.

Li, C. Y. and Mu, M. Q.: El Niño occurrence and sub-surface ocean temperature anomalies in the Pacific warm pool, Chinese Journal of Atmospheric Sciences (in Chinese), 23(5), 513-521, 1999.

Li, C. Y. and Mu, M. Q.: Relationship between East Asian winter monsoon, warm pool situation and ENSO cycle, Chin. Sci. Bull., 45(16), 1448-1455, doi:10.1007/BF02898885, 2000.

Li, C. Y. and Mu, M. Q.: The influence of the Indian Ocean dipole on atmospheric circulation and climate. Adv. Atmos. Sci., 18(5), 831-843. doi:10.1007/BF03403506, 2001.

Li, C. Y.: A Further Study of the Essence of ENSO, Climate and Environmental Research (in Chinese), 7(2), 160-174, 2002.

Li, C. Y., Mu, M. Q., and Pan, J.: Indian Ocean temperature dipole and SSTA in the equatorial Pacific Ocean, Chin. Sci. Bull., 47(3), 236-239, doi:10.1360/02tb9056, 2002.

Li, T., Wang, B., Chang, C. P. and Zhang, Y.: A theory for the Indian Ocean dipole-zonal mode, J. Atmos. Sci., 60(17): 2119-2135, doi: 10.1175/1520-0469(2003)060<2119:atftio>2.0.co;2, 2003.

Li, C. Y., Mu, M., Zhou, G. Q. and Yang, H.: Mechanism and prediction studies of the ENSO, Chinese Journal of Atmospheric Sciences (in Chinese), 32(4), 761-781, 2008.

Liu, H., Lin, P., Yu, Y. and Zhang, X.: The baseline evaluation of LASG/IAP Climate system Ocean Model (LICOM) version 2, Acta. Meteor. Sin., 26(3), 318-329, doi:10.1007/s13351-012-0305-y, 2012.

Lian, T., Chen, D. K., Tang, Y. M., Jin, B. G.: A theoretical investigation of the tropical Indo-Pacific tripole mode, Sci. China-Earth Sci., 57, 174-188, doi: 10.1007/s11430-013-4762-7, 2014.

Li, X. and Li, C. Y.: The tropical pacific–indian ocean associated mode simulated by licom2.0, Adv. Atmos. Sci., 34(12), 1426-1436, doi:10.1007/s00376-017-6176-5, 2017.

Li, C. Y., Li, X., Yang, H., Pan, J. and Li, G.: Tropical Pacific-Indian Ocean Associated Mode and Its Climatic Impacts Chinese Journal of Atmospheric Sciences (in Chinese), 42(3), 505-523, 2018.

Mu, M. and Duan, W. S.: A new approach to studying ENSO predictability: Conditional nonlinear optimal perturbation, Chin. Sci. Bull., 48(10), 1045-1047, doi:10.1007/BF03184224, 2003.

Mu, M., Duan, W. S. and Wang, B.: Season-dependent dynamics of nonlinear optimal error growth and El Niño-Southern Oscillation predictability in a theoretical model, Journal of Geophysical Research: Atmospheres, 112(D10), doi:10.1029/2005JD006981, 2007.

North G. R., Bell, T. L., Cahalan, R. F., Moeng, F. J.: Sampling errors in the estimation of empirical orthogonal functions, Mon. Wea. Rev., 110, 699-706, doi: 10.1175/1520-0493(1982)110<0699:seiteo>2.0.co;2, 1982.

Philander, S. G. H., Yamagata, T. and Pacanowski, R. C.: Unstable Air-Sea Interactions in the Tropics, J. Atmos. Sci., 41(4), 604-613, doi: 10.1175/1520-0469(1984)041<0604:UASIIT>2.0.CO;2, 1984.

Rasmusson, E. M. and Wallace, J. M.: Meteorological aspects of the El Niño/Southern Oscillation, Science, 222(4629), 1195-1202, doi:10.1126/science.222.4629.1195, 1983.

Ropelewski, C. F. and Halpert, M. S.: Global and regional scale precipitation patterns associated with the El Niño/southern Oscillation, Mon. Wea. Rev., 115(8), 1606-1626, doi:10.1175/1520-0493(1987)1152.0.CO;2, 1987.

Rayner, N. A., Parker, D. E., Horton, E. B., Folland, C. K., Alexander, L. V., Rowell, D. P., Kent, E. C. and Kaplan, A.: Global analyses of sea surface temperature, sea ice, and night marine air temperature since the late nineteenth century, J. Geophys. Res., 108(D14), 4407 doi:10.1029/2002JD002670, 2003.

Rao, S. A., Masson, S., Luo, J. J., Behera, S. K. and Yamagata, T.: Termination of indian ocean dipole events in a coupled general circulation model, J. Climate, 20(13), 3018-3035, doi:10.1175/JCLI4164.1, 2007.

Suarez, M. J. and Schopf, P. S.: A delayed action oscillator for ENSO, J. Atmos. Sci., 45(21), 3283-3287, doi: 10.1175/1520-0469(1988)045<3283:adaofe>2.0.co;2, 1988.

Saji, N. H., Coswami, B. N., Vinayachandran, P. N. and Yamagata, T.: A dipole in the tropical Indian Ocean, Nature, 401(6751), 360-363, doi:10.1038/43854, 1999.

Shen, X. S., Kimoto, M., Sumi, A., Numaguti, A. and Matsumoto, Jun.: Simulation of the 1998 East Asian Summer Monsoon by the CCSR/NIES AGCM. J Meteor Soc Japan, 79(3), 741-757, doi:10.2151/jmsj.79.741, 2001.

Saji, N. H. and Yamagata, T.: Possible impacts of Indian Ocean dipole mode events on global climate, Climate Research, 25(2), 151-169, doi: 10.3354/cr025151, 2003.

Taylor, K. E.: Summarizing multiple aspects of model performance in a single diagram, Journal of Geophysical Research: Atmospheres, 106(D7), 7183-7192, doi:10.1029/2000jd900719, 2001.

Ueda, H. and Matsumoto, J.: A possible triggering process of East–West asymmetric anomalies over the Indian Ocean in relation to 1997/98 El Niño, J. Meteor. Soc. Japan, 78(6), 803-818, doi:10.2151/jmsj1965.78.6_803, 2000.

Wyrtki, K.: El Niño-The Dynamic Response of the Equatorial Pacific Ocean to Atmospheric Forcing, J. Phys. Oceanogr., 5(4), 572-584, doi:10.1175/1520-0485(1975)005<0572:entdro>2.0.co;2, 1975.

Webster, P. J. and Yang, S.: Monsoon and ENSO: Selectively interactive systems. Quart. J. Roy. Meteor. Soc., 118(507), 877-926, doi:10.1002/qj.49711850705, 1992.

Webster, P. J., Moore, A. M., Loschnigg, J. P. and Leben R. R.: Coupled ocean-atmosphere dynamics in the Indian Ocean during 1997-98, Nature, 401(6751), 356-360, doi: 10.1038/43848, 1999.

Wang, X. and Wang, C. Z.: Different impacts of various El Niño events on the Indian Ocean Dipole, Climate Dyn., 42(3-4), 991-1005, doi: 10.1175/JCLI-D-12-00638.1, 2014.

Yu, L. S. and Rienecker, M. M.: Mechanisms for the Indian Ocean warming during the 1997-98 El Niño, Geophys. Res. Lett., 26(6), 735-738, doi:10.1029/1999GL900072, 1999.

Yang, H. and Li, C. Y.: Effect of the Tropical Pacific-Indian Ocean Temperature Anomaly Mode on the South Asia High, Chinese Journal of Atmospheric Science (in Chinese), 29(1): 99-110, 2005.

Yang, H., Jia, X. L. and Li, C. Y.: The tropical Pacific-Indian Ocean temperature anomaly mode and its effect, Chin. Sci. Bull., 51(23): 2878-2884, doi:10.1007/s11434-006-2199-5, 2006.

Yang, M., Li, X., Zuo, R., Chen, X. and Wang, L.: Climatology and Interannual Variability of Winter North Pacific Storm Track in CMIP5 Models, Atmosphere, 9(3), 79, doi:10.3390/atmos9030079, 2018.

Zhou, G. Q. and Zeng, Q. C.: Predictions of ENSO with a coupled atmosphere–ocean general circulation model, Adv. Atmos. Sci., 18(4), 587-603, doi:10.1007/s00376-001-0047-8, 2001.

Zheng, F., Zhu, J. and Zhang, R. H.: The impact of altimetry data on ENSO ensemble initializations and predictions, Geophys. Res. Lett., 34(13), doi:10.1029/2007gl030451, 2007.

Zheng, X. T., Xie, S. P., Du, Y., Liu, L., Huang, G. and Liu, Q.: Indian Ocean Dipole Response to Global Warming in the CMIP5 Multimodel Ensemble, J. Climate, 26(16), doi:6067-6080, 10.1175/JCLI-D-12-00638.1, 2013.

Zheng, C. W. and Li, C. Y.: Variation of the wave energy and significant wave height in the China Sea and adjacent waters. Renewable and Sustainable Energy Reviews, 43, 381-387, doi:10.1016/j.rser.2014.11.001, 2015.

Zheng, C. W. and Li, C. Y.: Propagation characteristic and intraseasonal oscillation of the swell energy of the Indian Ocean, Applied Energy, 197, 342-353, doi:10.1016/j.apenergy.2017.04.052, 2017.